coatings

MDPI

Article

First Principles Study of Atomic Oxygen Adsorption on Austenitic Stainless Steels Surfaces: A Theoretical Study

Xinghua Zhu [1], Zhou Liu [1], Qingguo Feng [1], Zhiyong Huang [2], Xiaoyang Zhu [2], Lei Xiao [2], Jianguo He [3], Ning Wang [4] and Yi Xu [1,*]

[1] Key Laboratory of Advanced Technologies of Materials, Ministry of Education, School of Materials Science and Engineering, Southwest Jiaotong University, Chengdu 610031, China
[2] Sichuan Liuhe Special Metal Materials, Co., Ltd., Mianyang 621700, China
[3] China Iron & Steel Research Institute Group, Beijing 100081, China
[4] Sichuan Haitaipu Technology, Co., Ltd., Mianyang 621700, China
* Correspondence: xybwbj@swjtu.cn

Abstract: The adsorption of atomic oxygen and surfaces is the starting point and key point to understand the oxidation process of stainless steel. Nowadays, numerous studies have focused on the metal composition of stainless steel, while the mechanism of non-metallic elements affecting atomic oxygen adsorption needs to be clarified. Here, adsorption of atomic oxygen on the surface of pure γ-Fe and H/N-containing austenitic stainless steels was investigated using first principles. We found that stable adsorption (>6 eV) can occur on pure γ-Fe and H/N-containing austenitic surfaces. In this process, the presence of hydrogen and nitrogen both enhance the adsorption of atomic oxygen, but their influence mechanisms are in opposition. Hydrogen enhances adsorption by breaking metal bonds near the surface, while nitrogen promotes adsorption by enhancing structural stability. The adsorption promotion of hydrogen (−6.7629 eV) is stronger than that of nitrogen (−6.6374 eV), but it can reduce the stability of the system. The introduction of appropriate nitrogen atoms may be beneficial to the improvement of corrosion resistance. This study provides valid data and a unique perspective on the erosion protection of atomic oxygen on austenitic surfaces.

Keywords: austenite; first principles; adsorption; atomic oxygen; stainless steel

Citation: Zhu, X.; Liu, Z.; Feng, Q.; Huang, Z.; Zhu, X.; Xiao, L.; He, J.; Wang, N.; Xu, Y. First Principles Study of Atomic Oxygen Adsorption on Austenitic Stainless Steels Surfaces: A Theoretical Study. *Coatings* **2023**, *13*, 455. https://doi.org/10.3390/coatings13020455

Academic Editor: Eduardo Guzmán

Received: 24 January 2023
Revised: 8 February 2023
Accepted: 14 February 2023
Published: 17 February 2023

1. Introduction

Stainless steel materials with excellent mechanical, processing and welding properties [1] are often used to build vacuum systems [2] and in aerospace applications [3]. However, they are often subject to atomic oxygen erosion when used in the low earth orbit environment because of the large amount of atomic oxygen present in this environment [4]. This erosion results in the formation of various oxides on the surface, which can change the surface properties.

Nowadays, the research on the oxidation process of stainless steel surfaces has been widely reported [5–8] and many encouraging results have been achieved. It has been recognized that oxidation begins with oxygen adsorption. The subsequent process is the nucleation, growth and coalescence of two-dimensional oxides. In these processes, the complex interaction between atomic oxygen and metal surfaces is the core. Oxygen adsorption at the long bridge site is generally considered to be more stable [9] than at other sites considered to be highly symmetrical in adsorption [10]. In addition, Tomasz Ossowski and Adam Kiejna [11] have shown that the adsorption of atomic oxygen at all highly symmetrical sites (pseudo threefold-hollow, long-bridge, short-bridge, on-top) is stable at both low (0.25 monolayer) and high (1 monolayer) coverage conditions. The electron is transferred from the surface Fe atom to the oxygen atom when the atomic oxygen interacts with the surface of stainless steel [9]. In fact, previous theoretical studies have shown that oxygen produces dissociative adsorption on the surface of iron [10]. The

adsorption of atomic oxygen is a non-activated process when the coverage rate is up to 1 monolayer [12], while the dissociation adsorption is non-activated when the coverage rate is lower (<0.5 monolayer) [12,13]. As adsorption proceeds, oxygen atoms tend to gather and begin to penetrate below the surface to form FeO. The penetration of more oxygen atoms leads to the gradual transformation of FeO into Fe_3O_4 [14]. However, the adsorption of atomic oxygen will be disturbed by other kinds of atoms. For instance, atomic oxygen is more likely to be trapped by Cr [15,16] because of the stronger electronegativity difference between oxygen and chromium [17]. Therefore, a common understanding is that the corrosion resistance of stainless steel stems from the chromium-rich oxide layer (theoretically composed of different oxides of iron and chromium and their mixtures, with the main component being Cr_2O_3 [18]), which acts as a barrier to prevent further diffusion of atomic oxygen into the material [19–21].

Many studies attribute the good corrosion resistance of stainless steel to Cr_2O_3 to the low diffusion constants of Cr and O [22–25]. Meanwhile, it has higher chemical stability compared to Fe oxides [26,27]. Chromium dominates the entire oxide layer at very low oxygen pressures (below 103 Pa) and temperatures above 350 °C [28–31]. These oxides can effectively improve the corrosion resistance of the alloy. For example, the contact surface on the nanometer scale presents a more uniform and compact shape when the clean surface of pre-oxidized FeCrNi alloy makes contact with water vapor. This dense Cr oxide barrier layer can prevent the further oxidation of Fe [8]. However, this can lead to many serious consequences. One consequence is the depletion of Cr content on the surface, which will greatly affect the surface performance. On the other hand, only iron oxide is formed on the surface at temperatures up to 400 °C, although not all Fe-Cr alloys follow this rule [32]. This means that the protective layer dominated by Cr is not always effective.

In fact, interstitial nonmetallic atoms such as nitrogen also affect the adsorption of atomic oxygen. These atoms can exist stably in the gap of FCC due to the small atomic radii. They can affect the oxidation process by causing local structural deformation and affecting the movement of electrons in the crystal. Hydrogen can be present in stainless steel in a variety of forms, such as an interstitial atom [33], owing to its small atomic radius. These hydrogen states can have many effects on the properties of the alloy such as hydrogen embrittlement [34]. In contrast, nitrogen can only obtain low mobility due to its large atomic radius. Similar to hydrogen, nitrogen can also exist in steel in the form of interstitial atoms. It is a very strong element for forming and stabilizing austenite [35,36]. It is well known that nitrogen alloying can significantly improve the pitting resistance of austenitic stainless steel despite its limited solubility. Ye et al. [37] believed that the rapid passivation and stabilization mechanism of the nitrogen-containing surface of austenitic stainless steel [38–41] is closely related to the improvement of adsorption capacity caused by the presence of N atoms. These atoms can change the properties of the local structure and thus affect the adsorption of atomic oxygen. Unfortunately, relevant studies are lacking.

In this work, we investigated the effect of interstitial atoms H and N on the adsorption of atomic oxygen using first principles. γ-Fe is used to represent austenitic stainless steel. Six control groups were set up to investigate the effect of interstitial atoms on atomic oxygen adsorption. In all models, spin polarization is included. The adsorption energy is used to analyze the interaction between atomic oxygen, and surface and cohesion energy is used to characterize the stability of the system. The electronic structure is analyzed by density of states (DOS), electron localization function (ELF) and crystal orbital Hamilton population (COHP). Atomic charges based on Mulliken's work is used to analyze charge transfer. This study provides valid data and a unique perspective on the erosion protection of atomic oxygen on austenitic surfaces.

2. Calculation Details

This work is based on the density functional theory (DFT) in the Vienna Ab-initio Simulation Package (VASP) [42]. The eight-layer face-centered cubic (FCC) structure with 144 atoms is used as an austenitic stainless steel. The interstitial atoms H and N are placed

in a second layer close to the surface before structure optimization. Atomic oxygen is placed in a vacuum layer above the interstitial atoms. The distance between atomic oxygen and the surface is within the van der Waals radius. After the pure austenite is fully relaxed, the fractional coordinates of the atoms in the lower five layers are fixed to represent the bulk phase, while the top three layers are allowed to relax. A vacuum layer of 15 Å is introduced in the c-axis direction to eliminate periodic effects. Adsorption energy (E_{ads}) and cohesive energy (E_{coh}) [43,44] are used to discuss the adsorption state and stability of the system, respectively, and the calculation formulas of these are as follows:

$$E_{ads} = E_{tot} - E_{sub} - E_{ao}$$

where E_{tot} is the total energy of the model, E_{sub} is the energy of the block without sorbent and E_{ao} is the energy of the atomic oxygen.

$$E_{coh} = \frac{1}{n}\left(E_{tot} - \sum x_A E_{atom}^A\right)$$

where n is the total number of atoms, E_{tot} is the total energy of the model, x_A is the number of atoms of type A and E_{atom}^A is the energy of an isolated type A atom.

Perdew-Burke-Ernzerhof (PBE) [45] exchange-correlation functional and Projector Augmented-Wave (PAW) [46,47] pseudopotential are used in this work. We use a cut-off energy of 500 eV to compute all models. Self-consistent field (SCF) convergence threshold is set to 1×10^{-5} eV/atom. The model of pure austenite was first fully relaxed. Then, all models were optimized for atomic positions, and the force on each ion was less than 0.02 eV/Å. The Grimme method of DFT-D3 [48] was used to correct the van der Waals forces between atomic oxygen and austenite. Spin polarization was also considered. A $2 \times 1 \times 1$ k-point grid in the Brillouin region was used in all models. VASPKIT [49] is used in the analysis of DOS. Visualization for Electronic and Structural Analysis (VESTA) [50] is used to draw the ELF [51]. Local-Orbital Basis Suite Towards Electronic-Structure Reconstruction (LOBSTER) [52–54] is used for COHP [55]. Atomic charges based on Mulliken's work [56] were used to analyze charge transfer.

3. Results and Discussion

First, the pure γ-Fe and austenite containing interstitial atoms H and N was calculated, and these models are shown in Figure 1. The cohesive energy is shown in Table 1.

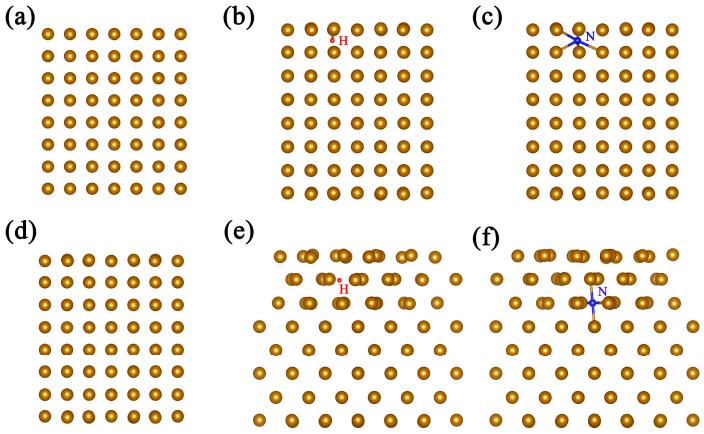

Figure 1. Models of pure γ-Fe and H/N-containing austenite. (**a**–**c**) are the models of pure γ-Fe and H/N-containing austenite before geometry optimization, respectively. (**d**–**f**) are the models of pure γ-Fe and H/N-containing austenite after geometry optimization, respectively.

Table 1. Cohesive energy of all models without atomic oxygen adsorption.

	E_{coh}/(eV/atom)
Pure γ-Fe	−4.4515
H-containing Fe	−4.4413
N-containing Fe	−4.4741

Both hydrogen and nitrogen atoms can be stably located at the gap of γ-Fe, but they are at different sites, as seen in Figure 1. The small atomic radius [17] allows the hydrogen atom to be trapped by the Fe atom. Turnbull and Hutchings [57] suggested that austenite is a trap for hydrogen capture. Although the trap effect in austenite is smaller than that of the austenite-ferrite interface, the existence of austenite makes the diffusion path provided by ferrite more tortuous. However, Turk et al. [58] argue that it is uncertain whether austenite can be treated simply as a point trap. It is undeniable that hydrogen can stably exist in the interior and surface of austenite and affect its properties, although the mechanism of hydrogen capture is controversial. On the contrary, the nitrogen atom is located in the octahedral gap in the FCC structure. It is able to interact with multiple nitrogen atoms to stabilize the FCC structure. This is demonstrated by an increase in cohesion energy, as seen in Table 1. These also have been confirmed by a large number of previous studies [33,35,36,59–61]. This octahedral interstitial atom can bring additional lattice distortion energy to the overall system [61], resulting in a significant increase in strength and corrosion resistance [62]. In fact, these nitrogen atoms can react with Cr to form a relatively stable interstitial nitride phase on the surface of stainless steel. They can act as kinetic barriers for alloy dissolution [63].

The DOS and ELF of pure γ-Fe and H/N-containing austenite are shown in Figures 2 and 3, respectively.

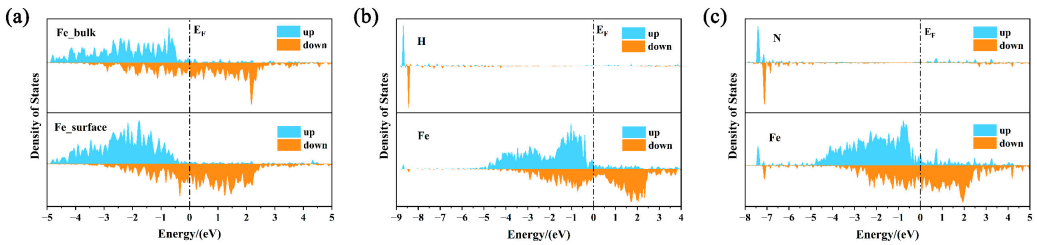

Figure 2. DOS of pure γ-Fe and H/N-containing austenite. (**a**–**c**) are the DOS of pure γ-Fe and H/N-containing austenite, respectively.

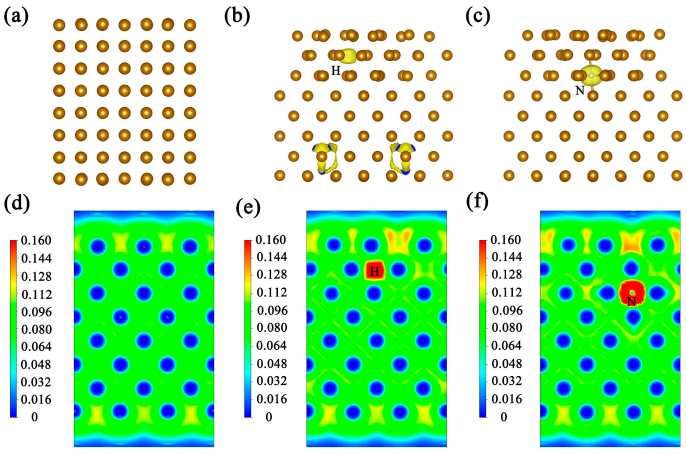

Figure 3. DOS of pure γ-Fe and H/N-containing austenite. (**a**–**c**) are the 3D ELF of pure γ-Fe and H/N-containing austenite, respectively. (**d**–**f**) are the 2D ELF of pure γ-Fe and H/N-containing austenite, respectively.

Both hydrogen and nitrogen doping cause charge enrichment, as shown in Figure 3b,c. The solitary electron property of hydrogen allows the charge inside the metal to be effectively bound around it, which can break the metal bonds in a localized environment. One consequence of this is that good ductility may be weakened near the local environment of the doping. The conclusion that a large amount of hydrogen is harmful to austenite has been proven by many previous works [34,64–66].

However, the nitrogen atoms located in the octahedral gap sites enhance the stability of the FCC structure. Although nitrogen doping can also cause lattice distortion in the local structure, the FCC structure is not damaged, which is consistent with previous studies [62,67–69]. The DOS also confirms these. In pure γ-Fe, the 3D orbitals of the internal Fe atom have good delocalization property in the energy range of −5 to 3 eV due to the internal crystal field, as seen in Figure 2a. On the contrary, the surface Fe atom has higher activity, which results in the occupied state of 3D electrons mainly in the energy range of −4 to 2 eV. The DOS of the Fe atom produces corresponding occupied states in the deep energy range of −7 to −9 eV after the interstitial atom was introduced, as seen in Figure 2b,c. It indicates that a chemical bond is formed between the interstitial atom and the Fe atom. In particular, for the nitrogen atom, its p-orbital undergoes a more pronounced dispersion.

Then, adsorption behavior of atomic oxygen on these model surfaces was calculated, and these models are shown in Figure 4. The adsorption energy, cohesive energy and Mulliken charge of atomic oxygen are shown in Table 2.

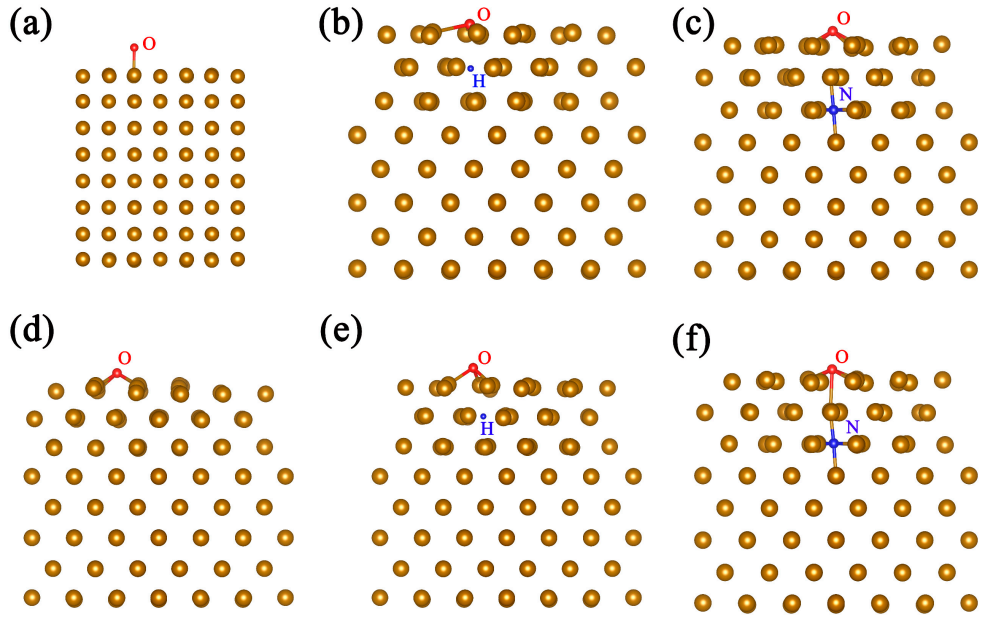

Figure 4. Model for the adsorption of atomic oxygen on pure γ-Fe and H/N-containing austenite. (**a**–**c**) are the models for the adsorption of atomic oxygen on pure γ-Fe and H/N-containing austenite before geometry optimization, respectively. (**d**–**f**) are the models for the adsorption of atomic oxygen on pure γ-Fe and H/N-containing austenite after geometry optimization, respectively.

Table 2. Adsorption energy, cohesive energy and Mulliken charge of atomic oxygen of all models.

	E_{ads}/(eV)	E_{coh}/(eV/atom)	Mulliken Charge of Atomic Oxygen/(e)
Pure γ-Fe with atomic oxygen	−6.1312	−4.7355	−0.69
H-containing Fe with atomic oxygen	−6.7629	−4.7242	−0.66
N-containing Fe with atomic oxygen	−6.6374	−4.7483	−0.69

When adsorption occurs, the atomic oxygen interacts with multiple iron atoms and stably adsorbs at the bridge site, as shown in Figure 4. This is consistent with the previous literature [9,10]. Numerous experimental studies have been conducted on the process of oxygen adsorption on iron surfaces. It is shown that oxygen atoms are adsorbed in the fourfold coordinated hollow sites of Fe (100) in the initial stage [70]. On this basis, a series of ordered structures were found. The c(2 × 2) superstructure is formed at 0.25 monolayer oxygen coverage [9,71]. They are then transformed into more complex structures under 0.33 monolayer coverage conditions, which are often oversimplified to a c(3 × 1) pattern [72]. Additional structures [73] have been proposed to explain the latter model because its mechanism is more complex. For higher coverage, iron oxide begins to form. In this progress, oxygen atoms tend to gather and begin to penetrate below the surface to form FeO. The penetration of more oxygen atoms leads to the gradual transformation of FeO into Fe_3O_4 [14]. However, these processes are interfered with by other kinds of atoms. As mentioned above, atomic oxygen is more likely to be trapped by Cr [15,16] because of the stronger electronegativity difference between oxygen and chromium [17]. The dense chromium oxide barrier formed by Cr and O prevents further oxidation of Fe [8]. This is generally considered as the mechanism of corrosion resistance of stainless steel. But one of the costs is the depletion of Cr content on the surface in the oxygen-rich environment.

Similar to the case of no sorbents, both hydrogen and nitrogen atoms can be stably located at the interstices of γ-Fe, but their positions are different, as seen in Figure 4. In all cases, the charge is always transferred from iron to atomic oxygen, which is consistent with the previous literature [9], as shown in Table 2. Strong charge transfer exists between austenite and atomic oxygen to form chemical bonds. The adsorption energy of atomic oxygen on pure γ-Fe is between the adsorption energy of the bridge site and the hollow site, as reported in Ye's work [37]. This situation is reasonable due to different parameter selection. The hydrogen atom can be stably located close to the surface, while the nitrogen atom will penetrate deep into the austenite in order to be stable. Similarly, the hydrogen atoms are in the interstices, while the nitrogen atoms are located in the octahedral sites. There is a difference in the effect on adsorption energy although they behave similarly. The hydrogen atoms can break the metal bonds of the local environment thus weakening the stability of the system. At the same time, the small atomic radius [17] allows it to be present close to the surface. The force of the crystal field on the surface electrons is weakened when the electrons in the doped region are attracted by hydrogen, which will lead to higher activity of the surface electrons. As a result, the atomic oxygen will be more tightly adsorbed on the surface, as seen in Table 2. The action mechanism of the nitrogen atom is the opposite to that of hydrogen. It is located further away from the surface than hydrogen, but it is able to stabilize the FCC structure [62,67–69]. Atomic oxygen makes it difficult for the surface to undergo more severe lattice distortions when the structure of several atomic layers near the surface is strengthened by nitrogen. In this progress, the enhanced internal structure will weaken the crystal field force on the surface electrons because the local charge is tightly bound inside, which is consistent with the previous literature [37]. According to Ye's report [37], the adsorption energy will increase along with the nitrogen content. Therefore, the mechanism of increasing adsorption energy may be one of the reasons for rapid passivation and stabilization of the passivation film on nitrogen-containing austenitic stainless steel [40,41]. In other words, the introduction of appropriate nitrogen atoms may contribute to the rapid passivation and stability of the surface passivation film, which is beneficial to the corrosion resistance. However, the adsorption of atomic oxygen is also closely related to the coverage. High density coverage will lead to the repulsive interaction between atoms, which can significantly reduce the adsorption energy [11]. Therefore, the content of interstitial atoms and the coverage rate of atomic oxygen should be considered comprehensively when studying the oxidation resistance of stainless steel.

The DOS, ELF and COHP of these models adsorbed with atomic oxygen are shown in Figures 5–7, respectively.

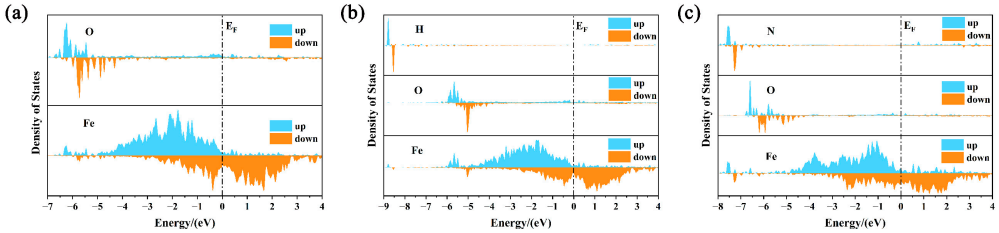

Figure 5. DOS of pure γ-Fe and H/N-containing austenite adsorbed with atomic oxygen. (**a**–**c**) are the DOS of pure γ-Fe and H/N-containing austenite adsorbed with atomic oxygen, respectively.

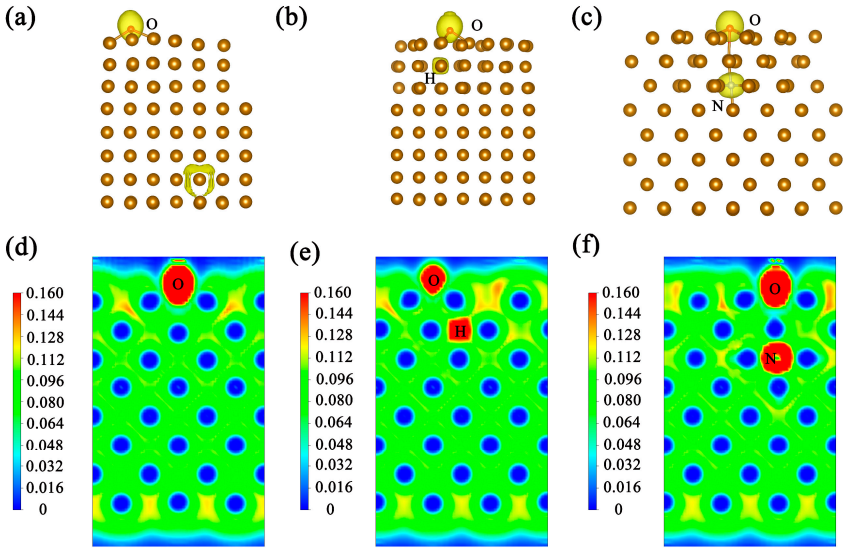

Figure 6. ELF of pure γ-Fe and H/N-containing austenite adsorbed with atomic oxygen. (**a**–**c**) are the 3D ELF of pure γ-Fe and H/N-containing austenite adsorbed with atomic oxygen, respectively. (**d**–**f**) are the 2D ELF of pure γ-Fe and H/N-containing austenite adsorbed with atomic oxygen, respectively.

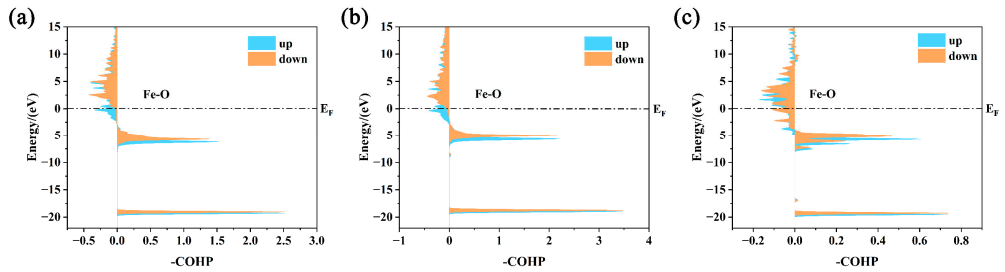

Figure 7. COHP of pure γ-Fe and H/N-containing austenite adsorbed with atomic oxygen. (**a**–**c**) are the COHP of pure γ-Fe and H/N-containing austenite adsorbed with atomic oxygen, respectively.

Figure 6d–f shows the charge enrichment caused by the doping of hydrogen and nitrogen and the adsorption of atomic oxygen. The DOS and COHP also confirmed these phenomena. Both oxygen and iron have corresponding occupied states in the energy range of −6.5 to −4.5 eV, as seen in Figure 6a–c. This indicates that the 2s orbital of oxygen and the 3d orbital of Fe overlap and form a chemical bond, which is consistent with previous studies [10,11]. At the same time, interstitial atoms and iron atoms have corresponding occupied states in the deep energy range of −7 to −9 eV. The 2s orbital of the oxygen atom becomes more dispersed in all cases because it can interact with multiple iron atoms, and this is also the case for the 2p orbital of the nitrogen atom. However, the 1s orbital of hydrogen is significantly spin polarized rather than dispersed because it only has one electron [17], as shown in Figure 5.

The peculiar one-electron structure of hydrogen atoms allows electrons from iron to accumulate around the hydrogen nucleus, which weakens the strength of the metal bonds within the crystal. The result is that the activity of the surface electrons increases due to the weakening of the crystal field force. On the contrary, nitrogen can enhance FCC stability, which has been demonstrated by a large number of studies [67–69]. The enhancement of internal local structure weakens the force between the surface and the interior. This also leads to increased activity of electrons on the surface. COHP confirmed this. As shown in COHP, the Fe-O bond in both the pure γ-Fe model and hydrogen-containing model has only anti-bonding components contributed by spin-up electrons, as seen in Figure 7a,b. On the contrary, the antibonding component is contributed by both the spin up and spin down electrons in the nitrogen-containing model. This is because nitrogen enhances the stability of the FCC structure, which makes the internal electrons tightly bound. This leads to the increased activity of electrons on the surface because the bonding between the interior and the surface is weakened. As a result, the system stability and adsorption energy increased. The phenomenon of nitrogen increasing adsorption energy has also been reported in the previous literature [37]. The mechanism of increasing adsorption energy may be one of the reasons for rapid passivation and stabilization of the passivation film on nitrogen-containing austenitic stainless steel [40,41].Therefore, the introduction of appropriate nitrogen atoms may contribute to the rapid passivation and stability of the surface passivation film, which is beneficial to the corrosion resistance.

4. Conclusions

In this study, we have investigated the adsorption of atomic oxygen on the surface of pure γ-Fe and H/N-containing austenitic stainless steels using first principles. The conclusions are summarized as follows:

(1) Atomic oxygen can be stably adsorbed on the surface of pure γ-Fe and H/N-containing austenitic because of huge adsorption energies (>6 eV);
(2) Both interstitial atoms H and N can enhance the adsorption of atomic oxygen on the surface, but their mechanism of action is in opposition. Hydrogen enhances adsorption by breaking metal bonds near the surface, while nitrogen enhances adsorption by enhancing structural stability;
(3) The enhancement effect of hydrogen on adsorption energy (−6.7629 eV) is stronger than that of nitrogen (−6.6374 eV), but hydrogen will lead to the decrease of the stability of the system;
(4) The introduction of appropriate nitrogen atoms may contribute to the rapid passivation and stability of the surface passivation film, which is beneficial to the corrosion resistance.

This study provides valid data and a unique perspective on the erosion protection of atomic oxygen on austenitic surfaces.

Author Contributions: Conceptualization, X.Z. (Xinghua Zhu) and Y.X.; Software, Q.F.; Data curation, X.Z. (Xinghua Zhu), Z.L. and L.X.; Funding acquisition, Y.X., N.W., X.Z. (Xiaoyang Zhu) and Z.H.; Investigation, X.Z. (Xinghua Zhu), Z.L. and J.H.; Resources, Q.F.; Writing—original draft preparation, X.Z. (Xinghua Zhu); Writing—review and editing, Y.X.; Supervision, Y.X.; Visualization, Y.X. and Z.H. All authors have read and agreed to the published version of the manuscript.

Funding: This work was supported by the Science and Technology on Reactor Fuel and Materials Laboratory, Key R&D projects in the field of high and new Technology of Sichuan Province (20ZDYF0490, 20ZDYF0236) and the National Key Project of Research and Development Program of China (2016YFB1100202). The authors thank the Sichuan Liuhe Special Metal Materials Co. LTD for financial support.

Institutional Review Board Statement: Not applicable.

Informed Consent Statement: Not applicable.

Data Availability Statement: The data presented in this study are available on request from the corresponding author.

Acknowledgments: The authors are grateful to Bowen Chen for the helpful discussion and constructive comments on the manuscript.

Conflicts of Interest: The authors declare no conflict of interest.

References

1. Verma, J.; Taiwade, R.V. Effect of welding processes and conditions on the microstructure, mechanical properties and corrosion resistance of duplex stainless steel weldments—A review. *J. Manuf. Process.* **2017**, *25*, 134–152. [CrossRef]
2. Vesel, A.; Mozetič, M.; Zalar, A. Oxidation of AISI 304L stainless steel surface with atomic oxygen. *Appl. Surf. Sci.* **2002**, *200*, 94–103. [CrossRef]
3. Boyer, R.R.; Cotton, J.D.; Mohaghegh, M.; Schafrik, R.E. Materials considerations for aerospace applications. *MRS Bull.* **2015**, *40*, 1055–1066. [CrossRef]
4. Reddy, M.R. Effect of low earth orbit atomic oxygen on spacecraft materials. *JMatS* **1995**, *30*, 281–307. [CrossRef]
5. Ma, L.; Lynch, B.; Wiame, F.; Maurice, V.; Marcus, P. Nanoscale early oxidation mechanisms of model FeCrNi austenitic stainless steel surfaces at room temperature. *Corros. Sci.* **2021**, *190*, 109653. [CrossRef]
6. Massoud, T.; Maurice, V.; Klein, L.H.; Seyeux, A.; Marcus, P. Nanostructure and local properties of oxide layers grown on stainless steel in simulated pressurized water reactor environment. *Corros. Sci.* **2014**, *84*, 198–203. [CrossRef]
7. Ma, L.; Wiame, F.; Maurice, V.; Marcus, P. New insight on early oxidation stages of austenitic stainless steel from in situ XPS analysis on single-crystalline Fe–18Cr–13Ni. *Corros. Sci.* **2018**, *140*, 205–216. [CrossRef]
8. Ma, L.; Pascalidou, E.-M.; Wiame, F.; Zanna, S.; Maurice, V.; Marcus, P. Passivation mechanisms and pre-oxidation effects on model surfaces of FeCrNi austenitic stainless steel. *Corros. Sci.* **2020**, *167*, 108483. [CrossRef]
9. Tan, X.; Zhou, J.; Peng, Y. First-principles study of oxygen adsorption on Fe(110) surface. *Appl. Surf. Sci.* **2012**, *258*, 8484–8491. [CrossRef]
10. Błoński, P.; Kiejna, A.; Hafner, J. Theoretical study of oxygen adsorption at the Fe(110) and (100) surfaces. *Surf. Sci.* **2005**, *590*, 88–100. [CrossRef]
11. Ossowski, T.; Kiejna, A. Oxygen adsorption on Fe(110) surface revisited. *Surf. Sci.* **2015**, *637–638*, 35–41. [CrossRef]
12. Błoński, P.; Kiejna, A.; Hafner, J. Oxygen adsorption on the clean and O-precovered Fe (110) and (100) surfaces. *J. Phys. Condens. Matter* **2007**, *19*, 096011. [CrossRef]
13. Błoński, P.; Kiejna, A.; Hafner, J. Dissociative adsorption of O_2 molecules on O-precovered Fe(110) and Fe(100): Density-functional calculations. *PhRvB* **2008**, *77*, 155424. [CrossRef]
14. Busch, M.; Gruyters, M.; Winter, H. FeO(111) formation by exposure of Fe(110) to atomic and molecular oxygen. *Surf. Sci.* **2006**, *600*, 2778–2784. [CrossRef]
15. Das, N.K.; Suzuki, K.; Takeda, Y.; Ogawa, K.; Shoji, T. Quantum chemical molecular dynamics study of stress corrosion cracking behavior for fcc Fe and Fe–Cr surfaces. *Corros. Sci.* **2008**, *50*, 1701–1706. [CrossRef]
16. Das, N.K.; Suzuki, K.; Ogawa, K.; Shoji, T. Early stage SCC initiation analysis of fcc Fe–Cr–Ni ternary alloy at 288 °C: A quantum chemical molecular dynamics approach. *Corros. Sci.* **2009**, *51*, 908–913. [CrossRef]
17. Haynes, W. *CRC Handbook of Chemistry and Physics*; CRC Press: Boca Raton, FL, USA, 2012; Volume 94.
18. Tang, J.E.; Halvarsson, M.; Asteman, H.; Svensson, J.E. Microstructure of Oxidised 304L Steel and the Effects of Surface Roughness on Oxidation Behaviour. In *High Temperature Corrosion and Protection of Materials*; Trans Tech Publications Ltd.: Wollerau, Switzerland, 2001.
19. Ishikawa, Y.; Yoshimura, T. Importance of the surface oxide layer in the reduction of outgassing from stainless steels. *J. Vac. Sci. Technol. A* **1995**, *13*, 1847–1852. [CrossRef]
20. Betz, G.; Wehner, G.K.; Toth, L.; Joshi, A. Composition-vs-depth profiles obtained with Auger electron spectroscopy of air-oxidized stainless-steel surfaces. *J. Appl. Phys.* **1974**, *45*, 5312–5316. [CrossRef]
21. Mathieu, H.J.; Landolt, D. An investigation of thin oxide films thermally grown in situ on Fe–24Cr and Fe–24Cr–11Mo by auger electron spectroscopy and X-ray photoelectron spectroscopy. *Corros. Sci.* **1986**, *26*, 547–559. [CrossRef]
22. Vesel, A.; Mozetic, M.; Drenik, A.; Hauptman, N.; Balat-Pichelin, M. High temperature oxidation of stainless steel AISI316L in air plasma. *Appl. Surf. Sci.* **2008**, *255*, 1759–1765. [CrossRef]
23. Cho, B.; Choi, E.; Chung, S.; Kim, K.; Kang, T.; Park, C.; Kim, B. A novel Cr_2O_3 thin film on stainless steel with high sorption resistance. *Surf. Sci.* **1999**, *439*, L799–L802. [CrossRef]
24. Huang, K.; Zhang, D.; Hu, M.; Hu, Q. Cr_2O_3/C composite coatings on stainless steel 304 as bipolar plate for proton exchange membrane fuel cell. *Energy* **2014**, *76*, 816–821. [CrossRef]
25. Adams, R.O. A review of the stainless steel surface. *J. Vac. Sci. Technol. A* **1983**, *1*, 12–18. [CrossRef]
26. Strehblow, H.-H. Passivity of Metals Studied by Surface Analytical Methods, a Review. *Electrochim. Acta* **2016**, *212*, 630–648. [CrossRef]
27. Maurice, V.; Marcus, P. Progress in corrosion science at atomic and nanometric scales. *Prog. Mater. Sci.* **2018**, *95*, 132–171. [CrossRef]

28. Ishikawa, Y.; Odaka, K. Reduction of outgassing from stainless surfaces by surface oxidation. *Vacuu* **1990**, *41*, 1995–1997. [CrossRef]
29. Kocijan, A.; Donik, Č.; Jenko, M. Electrochemical and XPS studies of the passive film formed on stainless steels in borate buffer and chloride solutions. *Corros. Sci.* **2007**, *49*, 2083–2098. [CrossRef]
30. Shibagaki, S.; Koga, A.; Shirakawa, Y.; Onishi, H.; Yokokawa, H.; Tanaka, J. Chemical reaction path for thin film oxidation of stainless steel. *Thin Solid Film.* **1997**, *303*, 101–106. [CrossRef]
31. Mandrino, D.; Godec, M.; Torkar, M.; Jenko, M. Study of oxide protective layers on stainless steel by AES, EDS and XPS. *Surf. Interface Anal.* **2008**, *40*, 285–289. [CrossRef]
32. Donik, Č.; Kocijan, A.; Grant, J.T.; Jenko, M.; Drenik, A.; Pihlar, B. XPS study of duplex stainless steel oxidized by oxygen atoms. *Corros. Sci.* **2009**, *51*, 827–832. [CrossRef]
33. Borchers, C.; Michler, T.; Pundt, A. Effect of Hydrogen on the Mechanical Properties of Stainless Steels. *Adv. Eng. Mater.* **2008**, *10*, 11–23. [CrossRef]
34. Whiteman, M.B.; Troiano, A.R. Hydrogen Embrittlement Of Austenitic Stainless Steel. *Corrosion* **2013**, *21*, 53–56. [CrossRef]
35. Byrnes, M.L.G.; Grujicic, M.; Owen, W.S. Nitrogen strengthening of a stable austenitic stainless steel. *Acta Metall.* **1987**, *35*, 1853–1862. [CrossRef]
36. Reed, R.P. Nitrogen in austenitic stainless steels. *JOM* **1989**, *41*, 16–21. [CrossRef]
37. Ye, F.; Wang, Y.; Xu, F.; Ke, T. Effects of Interstitial Nitrogen Atoms on Atomic Oxygen Adsorption on Fe (001) Surface from Ab Initio Calculations. *Mater. Sci. Forum* **2017**, *898*, 849–855. [CrossRef]
38. Grabke, H.J. The Role of Nitrogen in the Corrosion of Iron and Steels. *ISIJ Int.* **1996**, *36*, 777–786. [CrossRef]
39. Jargelius-Pettersson, R.f.a. Electrochemical investigation of the influence of nitrogen alloying on pitting corrosion of austenitic stainless steels. *Corros. Sci.* **1999**, *41*, 1639–1664. [CrossRef]
40. Baba, H.; Kodama, T.; Katada, Y. Role of nitrogen on the corrosion behavior of austenitic stainless steels. *Corros. Sci.* **2002**, *44*, 2393–2407. [CrossRef]
41. Lei, M.K.; Zhu, X.M. Role of Nitrogen in Pitting Corrosion Resistance of a High-Nitrogen Face-Centered-Cubic Phase Formed on Austenitic Stainless Steel. *J. Electrochem. Soc.* **2005**, *152*, B291. [CrossRef]
42. Kresse, G.; Furthmüller, J. Efficiency of ab-initio total energy calculations for metals and semiconductors using a plane-wave basis set. *Comput. Mater. Sci.* **1996**, *6*, 15–50. [CrossRef]
43. Ding, Y.; Wang, Y. Unusual structural and electronic properties of porous silicene and germanene: Insights from first-principles calculations. *Nanoscale Res. Lett.* **2015**, *10*, 13. [CrossRef]
44. Bai, H.; Zhu, Y.; Qiao, W.; Huang, Y. Structures, stabilities and electronic properties of graphdiyne nanoribbons. *RSC Adv.* **2011**, *1*, 768–775. [CrossRef]
45. Perdew, J.P.; Burke, K.; Ernzerhof, M. Generalized Gradient Approximation Made Simple. *Phys. Rev. Lett.* **1996**, *77*, 3865–3868. [CrossRef]
46. Blöchl, P.E. Projector augmented-wave method. *PhRvB* **1994**, *50*, 17953–17979. [CrossRef]
47. Kresse, G.; Joubert, D. From ultrasoft pseudopotentials to the projector augmented-wave method. *PhRvB* **1999**, *59*, 1758–1775. [CrossRef]
48. Grimme, S.; Antony, J.; Ehrlich, S.; Krieg, H. A consistent and accurate ab initio parametrization of density functional dispersion correction (DFT-D) for the 94 elements H-Pu. *J. Chem. Phys.* **2010**, *132*, 154104. [CrossRef]
49. Wang, V.; Xu, N.; Liu, J.-C.; Tang, G.; Geng, W.-T. VASPKIT: A user-friendly interface facilitating high-throughput computing and analysis using VASP code. *Comput. Phys. Commun.* **2021**, *267*, 108033. [CrossRef]
50. Momma, K.; Izumi, F. VESTA 3 for three-dimensional visualization of crystal, volumetric and morphology data. *J. Appl. Crystallogr.* **2011**, *44*, 1272–1276. [CrossRef]
51. Becke, A.D.; Edgecombe, K.E. A simple measure of electron localization in atomic and molecular systems. *J. Chem. Phys.* **1990**, *92*, 5397–5403. [CrossRef]
52. Deringer, V.L.; Tchougréeff, A.L.; Dronskowski, R. Crystal Orbital Hamilton Population (COHP) Analysis As Projected from Plane-Wave Basis Sets. *J. Phys. Chem. A* **2011**, *115*, 5461–5466. [CrossRef]
53. Maintz, S.; Deringer, V.L.; Tchougréeff, A.L.; Dronskowski, R. Analytic projection from plane-wave and PAW wavefunctions and application to chemical-bonding analysis in solids. *J. Comput. Chem.* **2013**, *34*, 2557–2567. [CrossRef]
54. Maintz, S.; Deringer, V.L.; Tchougréeff, A.L.; Dronskowski, R. LOBSTER: A tool to extract chemical bonding from plane-wave based DFT. *J. Comput. Chem.* **2016**, *37*, 1030–1035. [CrossRef]
55. Dronskowski, R.; Bloechl, P.E. Crystal orbital Hamilton populations (COHP): Energy-resolved visualization of chemical bonding in solids based on density-functional calculations. *J. Phys. Chem.* **1993**, *97*, 8617–8624. [CrossRef]
56. Mulliken, R.S. Electronic Population Analysis on LCAO-MO Molecular Wave Functions. IV. Bonding and Antibonding in LCAO and Valence-Bond Theories. *J. Chem. Phys.* **1955**, *23*, 2343–2346. [CrossRef]
57. Turnbull, A.; Hutchings, R.B. Analysis of hydrogen atom transport in a two-phase alloy. *Mater. Sci. Eng. A* **1994**, *177*, 161–171. [CrossRef]
58. Turk, A.; Pu, S.D.; Bombač, D.; Rivera-Díaz-del-Castillo, P.E.J.; Galindo-Nava, E.I. Quantification of hydrogen trapping in multiphase steels: Part II—Effect of austenite morphology. *Acta Mater.* **2020**, *197*, 253–268. [CrossRef]

59. Mingolo, N.; Tschiptschin, A.P.; Pinedo, C.E. On the formation of expanded austenite during plasma nitriding of an AISI 316L austenitic stainless steel. *Surf. Coat. Technol.* **2006**, *201*, 4215–4218. [CrossRef]
60. Xu, X.; Wang, L.; Yu, Z.; Qiang, J.; Hei, Z. Study of microstructure of low-temperature plasma-nitrided AISI 304 stainless steel. *MMTA* **2000**, *31*, 1193–1199. [CrossRef]
61. Oda, K.; Kondo, N.; Shibata, K. X-ray Absorption Fine Structure Analysis of Interstitial (C, N)-Substitutional (Cr) Complexes in Austenitic Stainless Steels. *ISIJ Int.* **1990**, *30*, 625–631. [CrossRef]
62. Li, T.; Chien, S.-C.; Ren, Z.; Windl, W.; Ernst, F.; Frankel, G.S. Understanding the efficacy of concentrated interstitial carbon in enhancing the pitting corrosion resistance of stainless steel. *Acta Mater.* **2021**, *221*, 117433. [CrossRef]
63. Marcus, P.; Bussell, M.E. XPS study of the passive films formed on nitrogen-implanted austenitic stainless steels. *Appl. Surf. Sci.* **1992**, *59*, 7–21. [CrossRef]
64. Murakami, Y.; Kanezaki, T.; Mine, Y.; Matsuoka, S. Hydrogen Embrittlement Mechanism in Fatigue of Austenitic Stainless Steels. *MMTA* **2008**, *39*, 1327–1339. [CrossRef]
65. Tsay, L.W.; Yu, S.C.; Huang, R.T. Effect of austenite instability on the hydrogen-enhanced crack growth of austenitic stainless steels. *Corros. Sci.* **2007**, *49*, 2973–2984. [CrossRef]
66. Barnoush, A.; Vehoff, H. Electrochemical nanoindentation: A new approach to probe hydrogen/deformation interaction. *Scr. Mater.* **2006**, *55*, 195–198. [CrossRef]
67. Berns, H.; Gavriljuk, V.; Shanina, B. Intensive Interstitial Strengthening of Stainless Steels. *Adv. Eng. Mater.* **2008**, *10*, 1083–1093. [CrossRef]
68. Shankar, P.; Sundararaman, D.; Ranganathan, S. Clustering and ordering of nitrogen in nuclear grade 316LN austenitic stainless steel. *J. Nucl. Mater.* **1998**, *254*, 1–8. [CrossRef]
69. Ledbetter, H.M.; Austin, M.W. Effects of carbon and nitrogen on the elastic constants of AISI type 304 stainless steel. *MSEng* **1985**, *70*, 143–149. [CrossRef]
70. Parihar, S.S.; Meyerheim, H.L.; Mohseni, K.; Ostanin, S.; Ernst, A.; Jedrecy, N.; Felici, R.; Kirschner, J. Structure of O/Fe(001)-p(1×1) studied by surface x-ray diffraction. *PhRvB* **2010**, *81*, 075428. [CrossRef]
71. Erley, W.; Ibach, H. Vibrational excitations and structure of oxygen on Fe(110). *Solid State Commun.* **1981**, *37*, 937–942. [CrossRef]
72. Hodgson, A.; Wight, A.; Worthy, G. The kinetics of O_2 dissociative chemisorption on Fe(110). *Surf. Sci.* **1994**, *319*, 119–130. [CrossRef]
73. Freindl, K.; Partyka-Jankowska, E.; Karaś, W.; Zając, M.; Madej, E.; Spiridis, N.; Ślęzak, M.; Ślęzak, T.; Wiśnios, D.; Korecki, J. Oxygen on an Fe monolayer on W(110): From chemisorption to oxidation. *Surf. Sci.* **2013**, *617*, 183–191. [CrossRef]